ACS OMEGA

Article

http://pubs.acs.org/journal/acsodf

Water-Soluble Colorimetric Amino[*bis*(ethanesulfonate)] Azobenzene pH Indicators: A UV−Vis Absorption, DFT, and $^{1}H-^{15}N$ NMR Spectroscopy Study

Maria A. Cardona,[†] Damjan Makuc,[‡] Konrad Szaciłowski,[∥] Janez Plavec,[‡,§] and David C. Magri*[,†]

[†]Department of Chemistry, Faculty of Science, University of Malta, Msida MSD 2080, Malta

[‡]Slovenian NMR Centre, National Institute of Chemistry, Hajdrihova 19, SI-1000 Ljubljana, Slovenia

[∥]Academic Centre of Materials and Nanotechnology, AGH University of Science and Technology, aleja Adama Mickiewicza 30, 30-059 Kraków, Poland

[§]EN-FIST Centre of Excellence, Trg Osvobodilne fronte 13, SI-1000 Ljubljana, Slovenia

Supporting Information

ABSTRACT: Water-soluble azobenzene derivatives containing amino[*bis*(ethanesulfonate)] groups are demonstrated as colorful pH indicators in water and on filter paper. Vibrant color changes were observed from yellow/orange to pink between pH 1 and 4, which are attributed to an intramolecular charge-transfer mechanism. The pK_as of the indicators range from 2.1 to 2.6. $^{1}H/^{1}H-^{15}N$ NMR studies in deuterium oxide reveal that the protonation of the azobenzene pH indicators occurs predominantly at the β-azo nitrogen atom, in agreement with the density functional theory calculations. Excellent selectivity for protons was confirmed in water over common biologically relevant metal ions. Studies in methanol, however, indicate that the pH indicator with a methoxy group *ortho* to the amino[*bis*(ethanesulfonate)] group facilitates the selective coordination of Cu^{2+} with a binding constant pβ_{Cu2+} of 4.6 ± 0.1. The indicators complement the existing library of azobenzene indicator dyes and may be useful for measuring the environmental pH at higher proton concentrations.

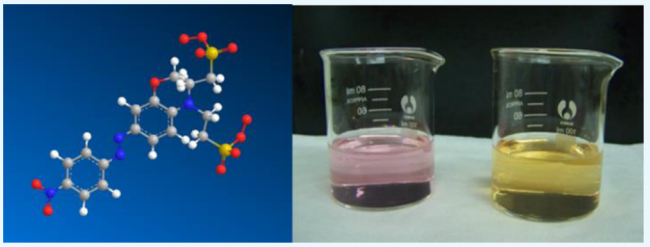

INTRODUCTION

Azobenzenes are a class of compound used as dyes for textiles, foods, soaps, and cosmetics, among many industrial uses.[1,2] Their relative ease of synthesis and photocontrollable *cis/trans* isomerization[3,4] make them useful components in smart materials,[5,6] metal−organic frameworks (MOFs),[7,8] self-assembled monolayers,[9,10] nonlinear optical materials,[11] and supramolecular devices.[12−16] Azobenzenes are also a classic scaffold for pH indicators and metal ion chemosensors.[17−24] In fact, the chromophore represents the largest percentage of commercially available pH indicators.[2] However, a majority of colorimetric azobenzene-based indicators and chemosensors are not so readily soluble in water and require an organic co-solvent.[25−30] Development of 100% water-soluble azobenzene indicators is thus most desirable. Furthermore, considering the abundance of azobenzene pH indicators, the choices are rather limited in the lower pH region. Previously, we reported the synthesis of a series of amino[*bis*(ethanesulfonate)] azobenzene pH indicators **3**−**5** with brilliant color changes and ideal water solubility properties (Figure 1).[31]

The motivation of this present study was to investigate the mechanism of protonation of these remarkable amino-[*bis*(ethanesulfonate)] azobenzene pH indicators in water. Aminoazobenzenes have been the subject of numerous studies by UV−vis absorption, ^{1}H NMR, and Raman spectroscopy over the past decades.[27−30,32] A common challenge has been to determine which of the two nitrogen atoms is preferentially protonated: the *p*-hybridized atom (Nγ) or the *s*-hybridized atom (Nβ) (Scheme 1). Pioneering work relied solely on UV−vis absorption spectroscopy for determining the tautomeric equilibrium.[33−35] More recent studies have relied on other spectroscopy techniques such as ^{1}H NMR and Raman, the majority of which were performed in organic solvents. However, the properties of aprotic solvents such as dimethyl sulfoxide (DMSO) and acetonitrile are significantly different than those of water. Hence, an objective was to gain direct insight into the protonation equilibrium of aminoazobenzene analogues in aqueous solution. We hypothesized that two-dimensional (2D) $^{1}H-^{15}N$ NMR techniques (Heteronuclear Multiple Bond Correlation (HMBC) and Heteronuclear Single Quantum Correlation (HSQC)) and density functional theory (DFT) calculations could be used to delineate the protonation equilibria in water.[36−41]

Herein, we report the physiochemical properties of the three water-soluble azobenzene pH indicators **3**−**5** (Figure 1). The indicators are water soluble on the account of the presence of

Received: June 28, 2017
Accepted: September 14, 2017
Published: September 26, 2017

DOI: 10.1021/acsomega.7b00887
ACS Omega 2017, 2, 6159−6166

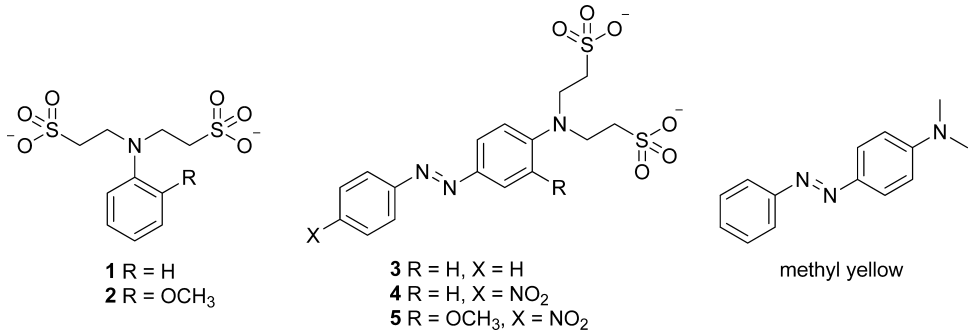

Figure 1. Molecules discussed in this study: model compounds **1** and **2**, the azobenzene pH indicators **3**–**5**, and methyl yellow.

Scheme 1. Generalized Protonation Mechanism for Aminoazobenzenes in Acidic Solution[1]

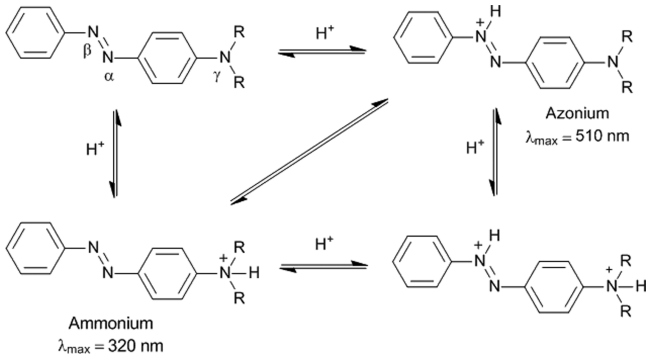

two ethanesulfonate groups attached to the amino nitrogen atom.[31,42,43] Using UV–vis absorption spectroscopy, we thoroughly characterize the acid–base properties of the indicators and compare them to the model compounds **1** and **2** and methyl yellow (Figure 1); using $^{1}H-^{15}N$ NMR spectroscopy and DFT calculations, we provide insight into the sites of protonation. To the best of our knowledge, this is the first study that examines the tautomeric equilibrium of azobenzene derivatives exclusively in water using UV–vis absorption spectroscopy in conjunction with 2D-NMR spectroscopic techniques and DFT calculations.

RESULTS AND DISCUSSION

The azobenzenes **3**–**5**, shown in Figure 1, were synthesized as reported in a preliminary study.[31] The alkylation of aniline and 2-methoxyaniline with sodium 2-bromoethanesulfonate gave **1** and **2**, which were further reacted with aniline or 4-nitroaniline via a diazonium coupling reaction. The products were characterized in detail by $^{1}H/^{13}C/^{15}N$ NMR, IR, and high-resolution mass spectrometry (HRMS) (refer to SI). The intermediates **1** and **2** were fully characterized as part of a separate study and included as model reference compounds.[42]

The azobenzenes **3**–**5** exhibit pH- and concentration-dependent color changes in water. Figure 2 shows the color changes of **3**–**5** over a range of concentrations (1 mM, 0.1 mM, and 10 μM). At 10 μM, the solutions of **3**–**5** are pinkish at pH 1.0 corresponding to a monoprotonated species. At pH 4.0, the solution of unprotonated **3** is yellow, whereas the solutions of **4** and **5** are orange. The color changes are attributed to an internal charge transfer mechanism resulting from the push–pull effect of the electron-donating amine and the electron-withdrawing nitro substituent.[11] At 0.1 mM, the protonated indicators exhibit red solutions at pH 1.0, whereas unprotonated **3**–**5** are yellow, red, and reddish-orange, respectively, at pH 4.0. Azobenzene **3** exhibits the broadest usable concen-

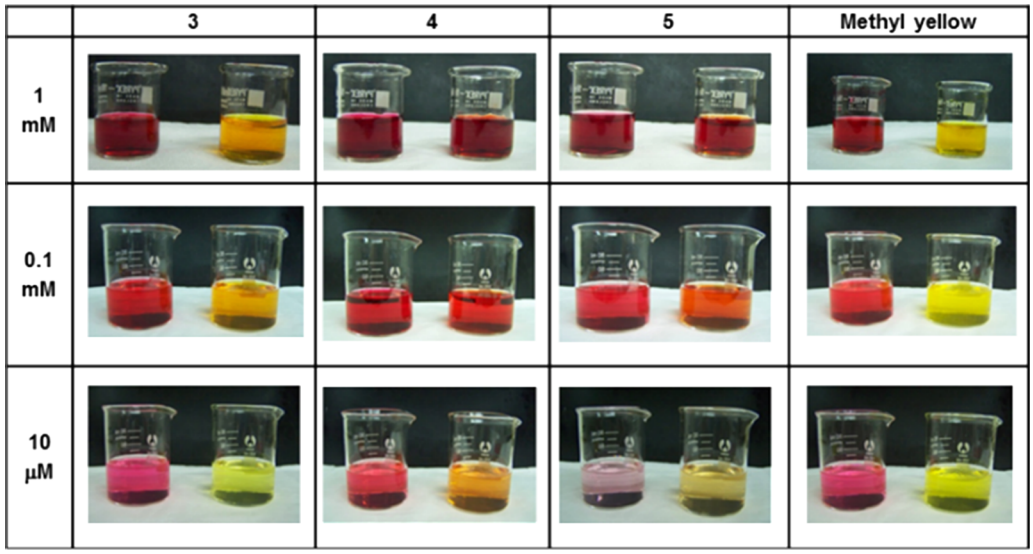

Figure 2. Azobenzene compounds **3**–**5** and methyl yellow at pH 1.0 (left beaker) and pH 4.0 (right beaker) in water. Methyl yellow was demonstrated in 1:4 (v/v) methanol/water due to the limited aqueous solubility. Adapted from ref 31.

DOI: 10.1021/acsomega.7b00887
ACS Omega 2017, 2, 6159–6166

tration range as a pH indicator between 1 μM and 1 mM, whereas **4** and **5** are most vibrant at a concentration of 10 μM.

The commercially available pH indicator methyl yellow (*N*,*N*-dimethyl-4-aminoazobenzene) was also examined at the same concentrations, for comparison, as shown in Figure 2. The observed color changes of methyl yellow resemble those of **3**. Methyl yellow was studied in 1:3 (v/v) MeOH/H_2O to ensure adequate solubility. The two sulfonate moieties within azobenzenes **3**−**5** allow for solubility in water at 10 mM concentrations. These observations are in agreement with the calculated octanol−water distribution coefficients (log *P*). The log *P* of methyl yellow is predicted to be 4.43. By contrast, the indicators **3**−**5** are soluble in water, in relatively good agreement with the calculated log *P* values of 0.21, 0.60, and 0.61, respectively.

UV−Vis Absorption Spectrophotometric Studies. The sulfonated compounds **1** and **2** and the azobenzenes **3**−**5** were thoroughly investigated as a function of pH and concentration by UV−vis absorption spectroscopy.[31,42] The UV−vis absorption spectra of **3**−**5** as a function of pH are shown in Figure 3. A summary of the spectroscopic parameters can be found in Table 1. Compounds **1** and **2** absorb below 300 nm and hence do not exhibit any color changes in water on titration with acid, whereas the azobenzenes **3**−**5** display bands extending into the visible region.

Azobenzene **3** exhibits broad absorption bands at 264 nm (log ε = 4.49) and 425 nm (log ε = 4.23) at neutral and basic pH conditions. Below pH 4, these peaks decrease incrementally with the concomitant formation of a strong absorption peak at 529 nm (log ε = 4.62). These changes correspond to a sigmoidal titration profile over two pH units between pH 1 and 3 with an isosbestic point at 469 nm.[31]

Similarly, **4** displays a strong intramolecular charge transfer band, but at a longer wavelength of 481 nm (log ε = 4.12) in neutral and basic conditions due to the nitro group in the para position to the azobenzene moiety. A weak absorption band is also present at 264 nm (log ε = 3.78). On the addition of acid up to pH 1, a new band with absorption peaks at 530 nm (log ε = 4.35) and 547 nm (log ε = 4.35) results at the expense of the broad peak at 481 nm. An isosbestic point is observed at 484 nm. The weak band at 280 nm decreases in intensity (log ε = 3.52) as a new band appears at 346 nm.

Azobenzene **5** with the methoxy group exhibits a significantly different spectral output. The absorption bands are observed at 269 nm (log ε = 4.30) and 436 nm (log ε = 4.07) at basic and neutral conditions. These bands decrease in intensity at greater than 10^{-4} M acid with the formation of new bands at 323 nm (log ε = 4.15) and 515 nm (log ε = 3.87). Three isosbestic points are observed at 299 nm, 365 nm, and 529 nm, as illustrated in Figure 3.

pH titrations were also performed with methyl yellow (4-(dimethylamino)azobenzene) (Figures S1 and S2). Under alkaline and neutral conditions, methyl yellow displays peaks at 260 nm (log ε = 3.81) and 450 nm (log ε = 4.20). On the addition of acid, both these peaks decrease and are eventually replaced with maxima at 320 nm and 514 nm (log ε = 4.40). Isosbestic points appear at 348 nm and 474 nm. The longer wavelength band ca. 530 nm is assigned to protonation at the Nβ, whereas the band appearing at around 320−346 nm is due to protonation at Nγ.[34] The extension of this interpretation to **3** would suggest that preferential protonation occurs at the Nβ, whereas there is an equilibrium between the ammonium and azonium form in aqueous solution in the case of **4** and **5**. The

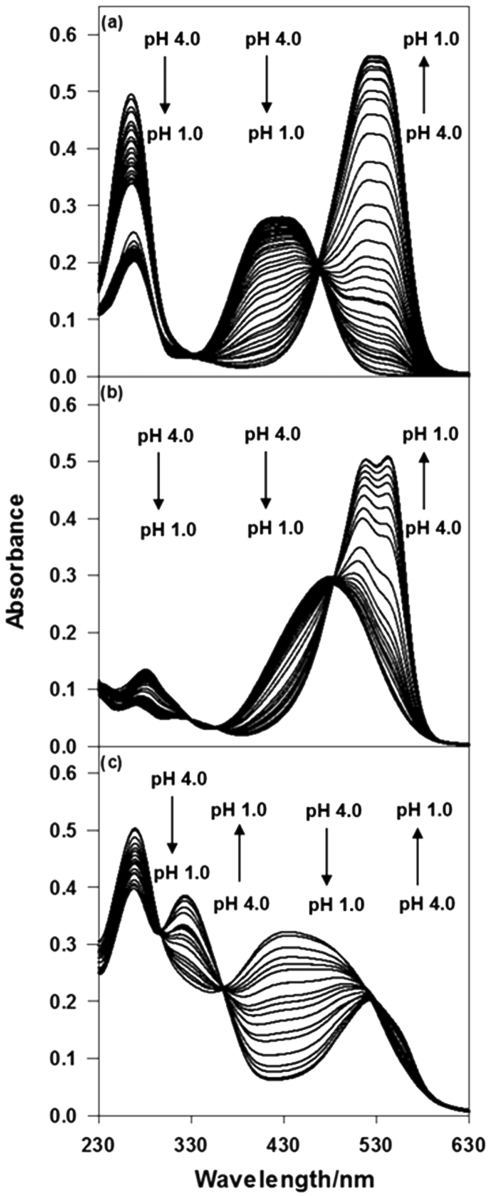

Figure 3. UV−vis absorption spectra of 20 μM **3** (a), 10 μM **4** (b), and 40 μM **5** (c) in water on titration with dilute HCl between pH 4.0 and 1.0. No changes were observed on further titration up to pH 13.[31]

shorter wavelength band was much more prominent with **5** than with **4**, implying that the equilibrium is shifted toward the azonium form in the case of **4**. However, the UV−vis absorption data alone does not provide conclusive evidence. Hence, further insight into the protonation equilibria was obtained by 2D $^{1}H-^{15}N$ NMR spectroscopy and DFT calculations (vide infra).

The practical application of **3**−**5** as pH test strips was examined by immersing 1 cm × 5 cm strips of filter paper in 0.1 M solutions of the respective indicator.[44] The addition of alkali solution onto the test strips results in yellow, brown-orange, and pink-violet colors for **3**−**5**, respectively. The tests strips changed color to pink in all three cases on the addition of acid (Figure 4). The results demonstrate the applicability of these azobenzene compounds as practical colorimetric pH indicators.

^{1}H NMR Titration Studies. The NMR spectra of compounds **1**−**5** were recorded in D_2O. In the case of **5**, the peaks were broad and unresolved, possibly due to aggregation.

DOI: 10.1021/acsomega.7b00887
ACS Omega 2017, 2, 6159−6166

Table 1. UV−Vis Absorption and Analytical Parameters of 10^{-5} M 1−5 in Water and Methyl Yellow in 1:3 (v/v) Methanol/Water

	1[a]	2[a]	3[b]	4[b]	5[b]	methyl yellow
pK_a[c]	3.1	4.2	2.2	2.1	2.6	3.2
$\lambda_{max.\ pH\ 7.0}$ (nm)	296	276	425	481	436	450
$\log \varepsilon_{\ pH\ 7.0}$[d]	3.20	3.41	4.23	4.12	4.07	4.20
$\lambda_{max.\ pH\ 1.0}$ (nm)	296	276	529	530	515	514
$\log \varepsilon_{\ pH\ 1.0}$	3.41	3.55	4.62	4.35	3.87	4.40
$DL_{pH\ 7.0}$ (nM)[e]			26	12	26	
$DL_{pH\ 1.0}$ (nM)[e]			6.9	3.3	18	
log P[f]	−1.89	−2.07	0.21	0.60	0.61	4.43

[a]Ref 42. [b]Ref 31. [c]Determined from the equation pH = pK_a + log $[(A_{max} - A)/(A - A_{min})]$. [d]Molar absorptivity ε in mol^{-1} L cm^{-1}. [e]The detection limit (DL) was determined using the equation DL = $3.3\sigma/S$, where σ is the standard deviation of the blank absorbance at the λ_{max} at pHs 1 and 7 for 10 blank samples and S is the slope of the calibration curve based on plots of the absorbance at λ_{max} for seven concentrations between 10 and 100 μM at pHs 1 (dilute HCl) and 7 (N-(2-hydroxyethyl)piperazine-N′-ethanesulfonic acid (HEPES) buffer). Good linearity was observed with R^2 > 0.997. [f]Log P values determined using Chemsketch product version 12.01.

Figure 4. Test strips of **3**−**5** (left to right) adsorbed on filter paper. The test strips on the left of each pair are treated with 0.01 M NaOH solution and the test strips on the right are treated with 0.01 M HCl.

Hence, the NMR spectra of **5** were subsequently recorded in DMSO-d_6 or mixed aqueous DMSO-d_6. The proton signals were assigned based on one- and two-dimensional NMR experiments including ^{1}H−^{13}C HMBC and ^{1}H−^{13}C HSQC spectra (see Supporting Information for the spectra). ^{1}H−^{15}N HMBC correlation spectroscopy was also performed to determine the absolute assignment of the nitrogen atoms (vide infra).[45−47]

Figure 5 illustrates the ^{1}H NMR spectra of **4** as a function of the increasing amount of dilute hydrochloric acid. At pD 10.1, the ^{1}H NMR spectrum of **4** exhibits two broad signals at δ_H 3.26 ppm and 3.89 ppm corresponding to the ethanesulfonate protons, and three doublets in the aromatic region at δ_H 6.82 ppm, 7.70 ppm, and 8.22 ppm. On an incremental addition of the acid, all of the proton signals are observed to undergo a downfield chemical shift. A chemical shift change ($\Delta\delta_H$) of 0.5 ppm is observed for the aromatic H4 and H8 atoms nearest the amino group, initially at 6.82 ppm at pD 10.1, whereas a much smaller change of $\Delta\delta_H \leq 0.1$ ppm is observed for the aromatic proton signals about the azo moiety and the more upfield ethylene protons adjacent to the sulfonates. Most notably, the doublet at 7.70 ppm resolves into two distinct peaks at pD 1.3.

Similar $\Delta\delta_H$ are observed on titrating **3** with acid in D_2O, although the chemical shift changes are not as dramatic as for **4**. No resonance shifts greater than 0.1 ppm are observed. However, **5** exhibits a striking $\Delta\delta_H$ near the amino group, similar to **3**, with the chemical shift changes up to 0.6 ppm. Due to limited solubility, the titration experiments of **5** had to be measured in a mixture of 1:1 or 4:1 (v/v) DMSO-d_6/D_2O. Methyl yellow also exhibited a large $\Delta\delta_H$ of 0.5 ppm for the aromatic hydrogen atoms adjacent to the amino nitrogen in 4:1 (v/v) DMSO-d_6/D_2O. A histogram of the ^{1}H NMR chemical shift data for compounds **3**−**5** and methyl yellow as a function of pD is given in Figure 6.

^{1}H−^{15}N NMR Titration Studies. ^{1}H−^{15}N gHMBC spectra of **3**−**5** and methyl yellow were obtained at pD 1 and pD 4 to gain insight into the site of nitrogen protonation in water (Table 2). ^{1}H−^{15}N gHMBC spectra of **3** are shown overlaid in Figure 7. Three nitrogen atom resonances are observed at pD 4. The large chemical shift changes observed on protonation are indicative of a significant redistribution of the electron density. Protonation of **3** yields a remarkable upfield chemical shift of 216 ppm for the azonium nitrogen atom Nβ, with a concomitant downfield shift of 45 ppm for the ammonium nitrogen atom Nγ. These chemical shifts can be rationalized by the predominant formation of the quinoid tautomer because protonation at the β-azo nitrogen atom results in a decrease in the N−N bond order and an increase in the C−N bond order at the ammonium nitrogen atom Nγ.[27] The α-azo nitrogen atom Nα also undergoes a noticeable upfield shift of 79 ppm. These results are in agreement with the previous studies that there is preferentially protonation at the β-azo nitrogen atom.[28] By comparison, the chemical shifts of methyl yellow in DMSO-d_6 are the same in direction, but less in magnitude.

Compound **4** exhibits four nitrogen atoms resonances, and the additional resonance due to the nitro moiety appears at 370 ppm independent of the acid concentration between pD 1 and 4. Furthermore, the α-azo nitrogen atom Nα undergoes an upfield shift of 39 ppm, whereas a downfield shift of 52 ppm was observed for the ammonium nitrogen atom Nγ. Obtaining a complete set of resonances for **5** proved difficult even in the presence of Cr^{3+}, which was added as a relaxant. The $\Delta\delta_N$ for **3** and **4** are quite significant for the β-azo nitrogen atom, with shifts of 216 nm and 243 ppm. The ^{15}N NMR results suggest that the protonation of **3** and **4** takes place predominantly at the β-azo nitrogen atom.

DFT Studies. DFT calculations were performed on **3**−**5** and methyl yellow at the b3lyp/6−31+g(d,p) level of theory (Figure 8).[48] The calculations were initially done in vacuum and with the sulfonate moieties protonated to achieve neutral molecules, thereby simplifying the analysis. Frontier molecular orbitals with the dianion species provide a more complex frontier orbital depiction as the charged sulfonate groups occupy a series of higher occupied molecular orbital (HOMO) levels. The HOMO-1 molecular orbitals, which describe the charge density of the lone electron pairs, are delocalized equally over the two central nitrogen atoms in all of the four cases, although it was not possible to differentiate which of the two diaza nitrogen atoms is the preferred site for protonation. The geometry of **5** has the aromatic plane perpendicular to the plane of the sulfonate groups, which is caused by a steric effect due to the close proximity of the methoxy substituent. Molecules **3** and **4** have a quasi-planar geometry.

A further simplification was to consider the ethyl derivative of **3**−**5** devoid of the sulfonate groups. This approach simplifies

DOI: 10.1021/acsomega.7b00887
ACS Omega 2017, 2, 6159−6166

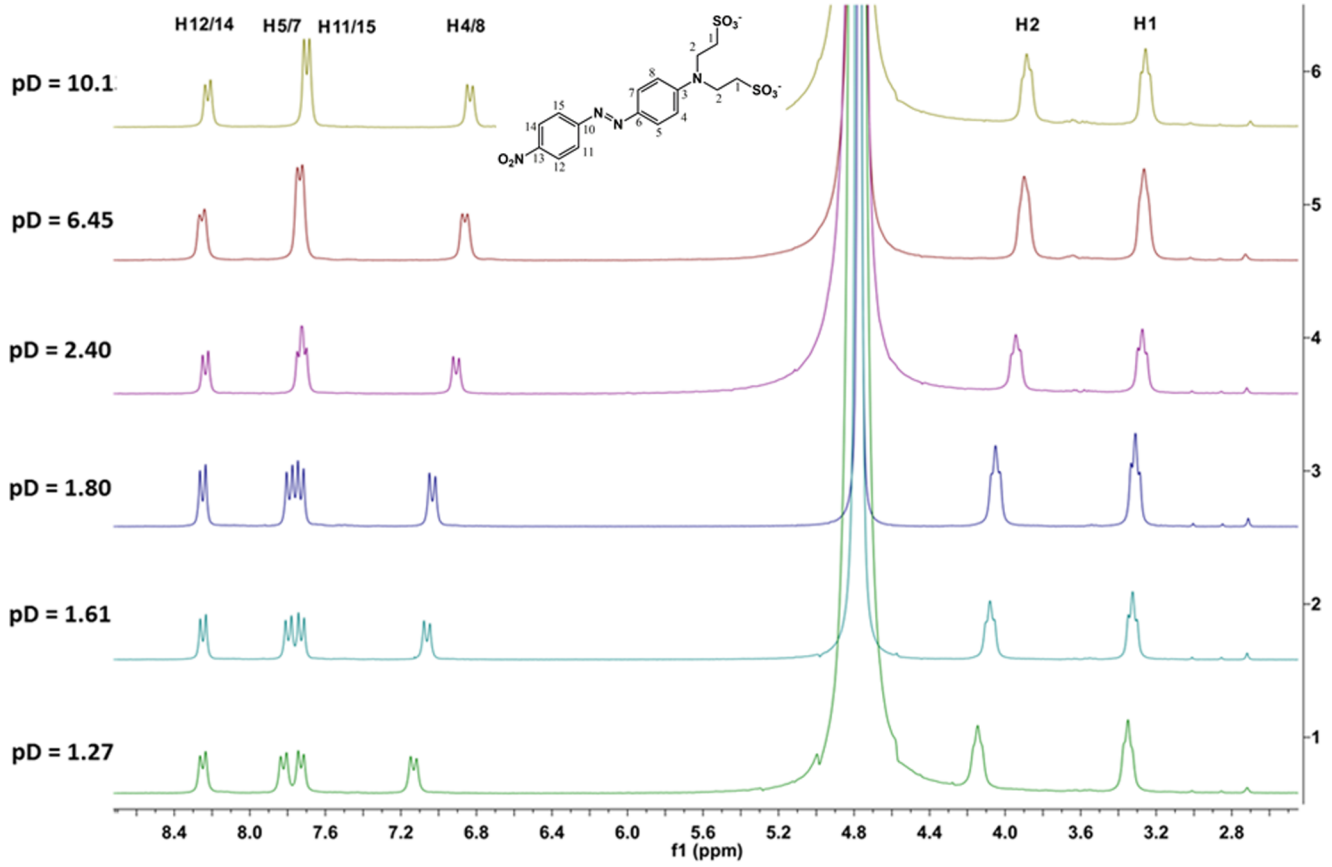

Figure 5. ^{1}H NMR spectra of **4** in D_2O as a function of added DCl.

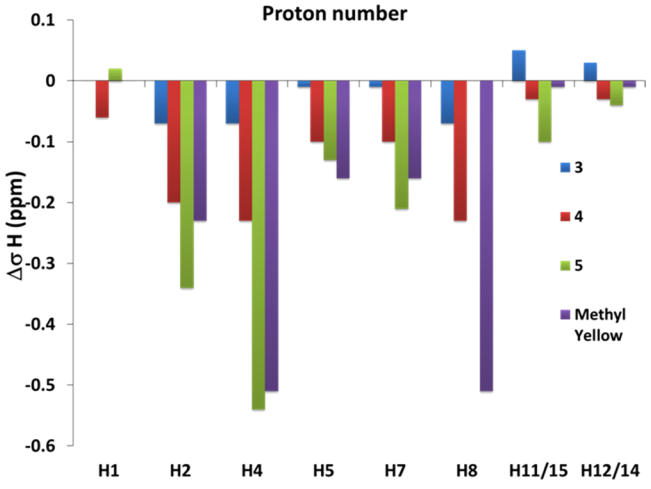

Figure 6. Selected ^{1}H NMR chemical shift changes for **3** and **4** in D_2O and **5** in 4:1 (v/v) DMSO-d_6/D_2O on titration from pD 10.1 to 1.3. Methyl yellow was measured in 4:1 (v/v) DMSO-d_6/D_2O.

the molecular charge analysis without affecting the electronic structure significantly. It was revealed that the lone pairs are almost equally distributed among the diaza nitrogen atoms, Nα and Nβ. However, in most cases, the middle nitrogen atom bears a slightly higher negative charge, except for the methoxy derivative **5**, in which the terminal nitrogen bears the highest negative charge. In vacuum or less polar solvents, the charge distribution within the diazo group depends on the local environment, which makes the unambiguous determination of the primary protonation site impossible. Furthermore, another pocket of negative charge at the methoxy and diethylamine sites supports copper binding as evident by a significant lone pair character in the HOMO orbital. The electrostatic and frontier orbital analysis were not fully conclusive in elucidation of the primary protonation site. Therefore, geometries and formation energies of all of the possible protonation isomers were calculated. These calculations clearly indicate that the terminal nitrogen atom of the diazo group is the favored protonation site. The differences in the total energies for the three protonated isomers is ca. 46 and 65 kJ mol^{-1} between the amino and middle nitrogen atoms, and the amino and terminal one, respectively. The difference between the two diaza nitrogen atoms, although not dramatic at 19 kJ mol^{-1}, clearly indicates a preference for protonation at the terminal nitrogen atom, Nβ.

Finally, the calculations for the sulfonated compounds were performed in water. The results are similar to those in vacuum. The protonation preferentially takes places at the Nβ nitrogen atom. The average energy difference for protonation at the Nβ atom versus protonation at the Nγ atom is 28 kJ mol^{-1} for **5** and methyl yellow, and 63 kJ mol^{-1} for **3** and **4**. By comparison, the energy difference between the Nα and Nβ nitrogen atoms is definitely smaller but still significant at 20−28 kJ mol^{-1}. The indicators **4** and **5** with the nitro substituent have the largest energy difference of 28 kJ mol^{-1}, whereas **3** and methyl yellow have the difference of 20 kJ mol^{-1}. Hence, the DFT calculations are in excellent agreement with the ^{1}H−^{15}N NMR spectroscopic studies. The thermodynamic calculations suggest that the protonation at Nβ yields the most stable forms. However, we cannot rule out that both nitrogen atoms may be involved in protonation, as they share common electron density clouds.

DOI: 10.1021/acsomega.7b00887
ACS Omega 2017, 2, 6159−6166

Table 2. ^{15}N Chemical Shifts (δ) of Compounds 3 and 4 in D_2O and 5 in 4:1 (v/v) DMSO-d_6/D_2O as a Function of pD[a]

	pD 1				pD 4			
compound	Nγ	Nα	Nβ	NO_2	Nγ	Nα	Nβ	NO_2
3[b]	120	402	238		75	481	454	
4	128	410	254	370	76	449	497	370
5	67(65)	[d]	(489)	370	65	[d]	[d]	369
methyl yellow[b,c]	86(78)	450(463)	369(398)		59	499	472	

[a] ^{15}N NMR δ were determined by ^{1}H−^{15}N correlations in gHMBC spectra. [b] The nitro substituent is absent. [c] ^{1}H−^{15}N gHMBC spectra recorded in DMSO-d_6. [d] Not observed. Values in parentheses measured in the presence of Cr^{3+} relaxant.

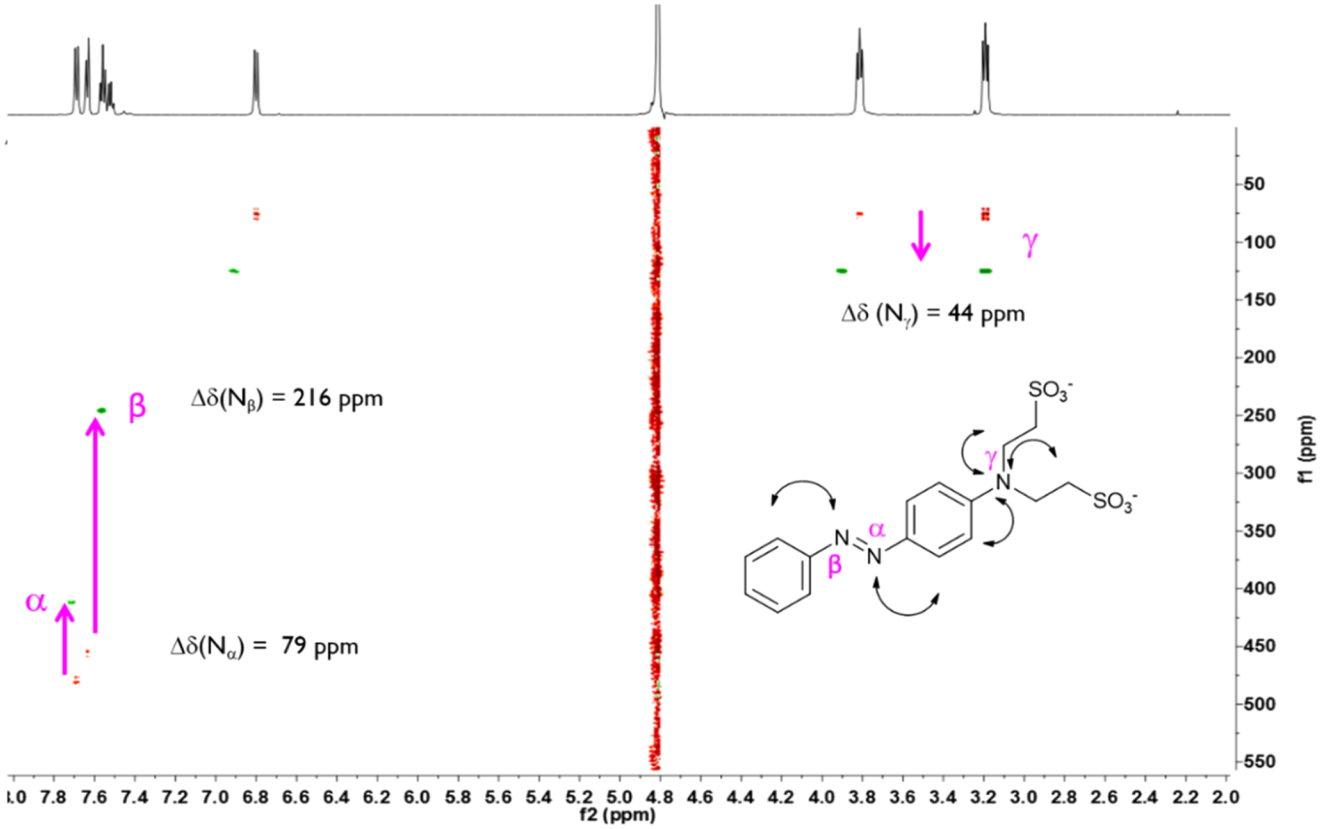

Figure 7. ^{1}H−^{15}N HMBC overlaid the spectra of **3** in D_2O. The red spots correspond to the ^{15}N chemical shifts at pD 4 and the green spots those at pD 1. Substantial nitrogen chemical shifts of 44 ppm, 79 ppm, and 216 ppm are observed for nitrogen atoms Nγ, Nα, and Nβ, respectively.

Metal-Binding Properties. The selectivity of **3**−**5** for a range of common metal ions in water was investigated in 20 mM HEPES buffered aqueous solution at a constant pH of 7.0 to avoid interference from protons. No significant color or UV−vis spectra changes were apparent on the addition of 0.2 mM Na^+, K^+, Ba^{2+}, Ca^{2+}, Mg^{2+}, Hg^{2+}, Fe^{3+}, Cu^{2+}, Zn^{2+}, Cr^{3+}, and Ce^{3+} added as chloride, perchlorate, or nitrate salts. These results confirm the inherent selectivity of the designed colorimetric indicators for H^+ in water.

Nonetheless, we did explore the coordination susceptibility of the azobenzene compounds with metal ions in methanol. We observed that the addition of 0.5 mM Cu^{2+} (1 equiv) to a solution of **5** gave rise to a bathochromic shift from 284 nm to 294 nm, with a slight increase in the intensity and a decrease in the band at 461 nm with an isosbestic point at 388 nm (Figure 9). A plot of the absorbance versus the pCu^{2+} in methanol at 461 nm yields a sigmoidal shaped curve over two log units. Fitting of the data provides a binding constant of $p\beta_{Cu2+}$ of 4.6 ± 0.1 (Figure S3). An analogous Cu^{2+}-sensitive iminodiacetate azobenzene chemosensor reported by Gunnlaugsson exhibited a $p\beta_{Cu2+}$ of 5.0 ± 0.1 in HEPES buffer at pH 7.[20] In both cases, the *ortho*-methoxy group is essential for Cu^{2+} coordination. By contrast, the addition of an equal amount of Cu^{2+} to **4**, which is devoid of the ortho-methoxy substituent, showed no significant changes in the UV−vis absorption spectra (Figure S4). In a previous study, a Job's plot analysis on the model compound **2** confirmed a 1:1 binding stoichiometry between Cu^{2+} and **2** in methanol.[42]

NMR titrations with 4 mM of **5** with 0.2 equiv of Cu^{2+} were performed in 2:1 (v/v) CD_3OD/D_2O. On addition of Cu^{2+}, the ^{1}H NMR spectrum of **5** broadens as expected due to the paramagnetic nature of Cu^{2+} (Figure 10). Peak broadening is most extensive near the aliphatic region of the spectra, particularly the resonance of the methoxy group at 4.05 ppm. The resonances of the protons nearest the sulfonates are also significantly broadened. The protons on the aromatic ring next to the amino nitrogen bearing the sulfonate groups are only slightly broadened, whereas the protons on the aromatic ring with the nitro group are much less affected. These findings give

DOI: 10.1021/acsomega.7b00887
ACS Omega 2017, 2, 6159−6166

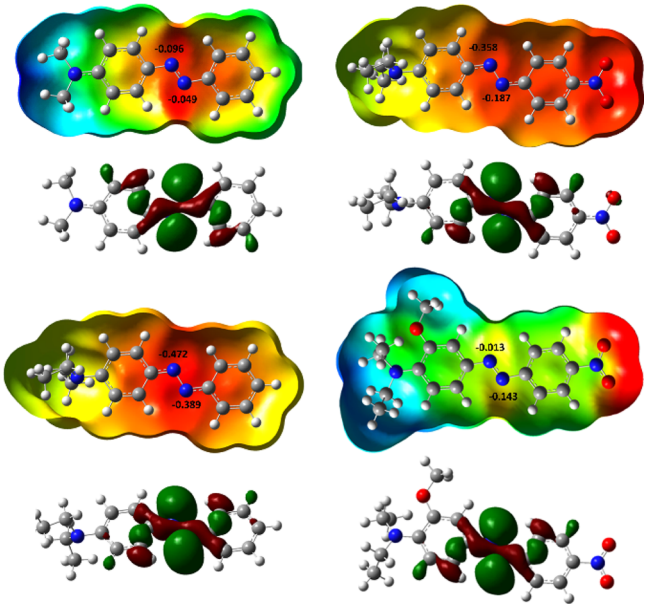

Figure 8. Distributions of the electrostatic potential and contours of HOMO-1 molecular orbitals for methyl yellow and three indicators (devoid of sulfonate groups) as calculated at the b3lyp/6−31++g(d,p) level of theory with the iefpcm solvation model included. Numbers indicate the Mullikan charges of the nitrogen atoms within the diazo functionality.

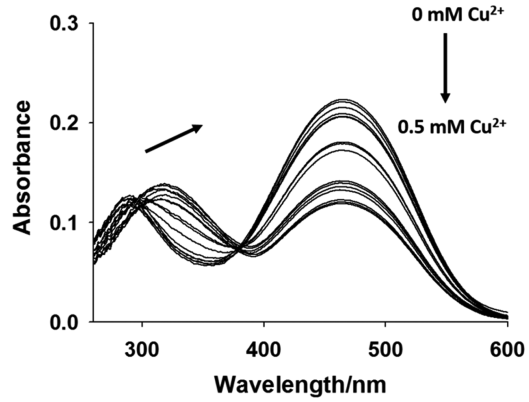

Figure 9. UV−vis absorption spectra of **5** in methanol on the addition of up to 0.5 mM Cu^{2+}. No change was observed in the aqueous solution.

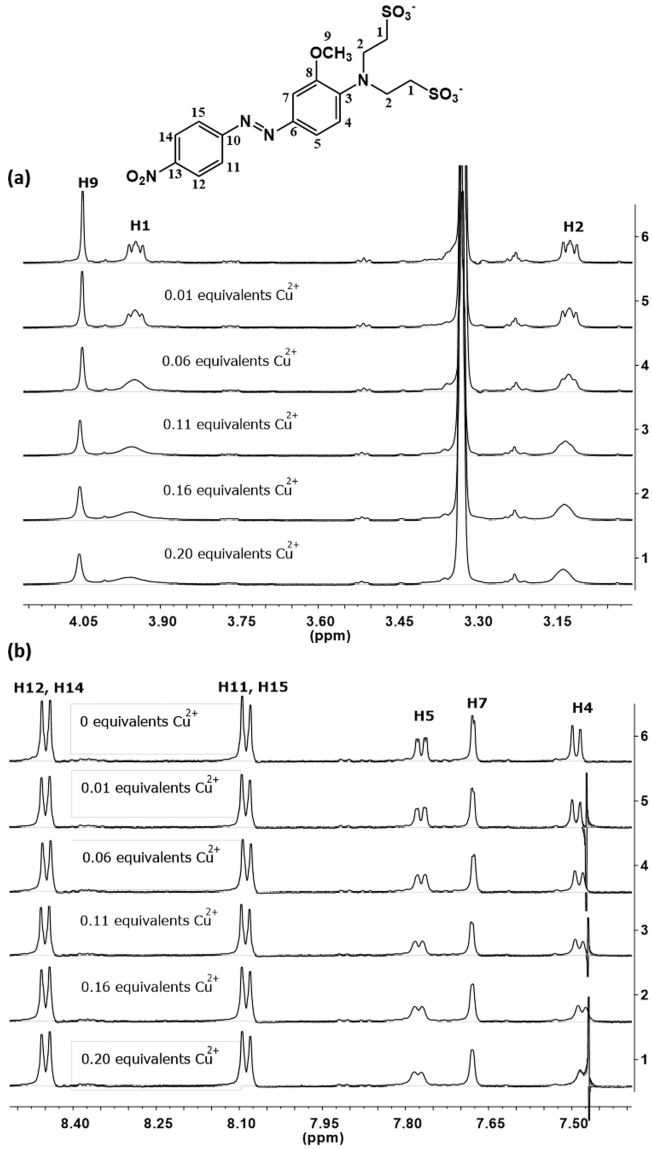

Figure 10. ^{1}H NMR spectra of 4.0 mM **5** in 4:1 (v/v) CD_3OD/D_2O on addition of up to 0.2 mM $CuCl_2$ (600 MHz): (a) the aliphatic region from 2.9 ppm to 4.2 ppm and (b) the aromatic region from 7.4 ppm to 8.5 ppm.

further confirmation that Cu^{2+} complexation occurs at the *o*-methoxy amino [*bis*(ethanesulfonate)] moiety.

CONCLUSIONS

In comparison to many commonly used azobenzene indicators, including methyl yellow, the azobenzene derivatives demonstrated here are readily soluble in 100% water up to millimolar concentrations. Selectivity studies in water confirm they function as pH indicators without interference from common biologically relevant metal ions. No evidence for coordination to the sulfonate groups is observed in water. Interpretation of the UV−vis absorption spectra suggests that protonation is principally at the terminal β-azo nitrogen atom, which is corroborated by in-depth $^{1}H-^{15}N$ 2D-NMR and DFT studies. Investigations in methanol provide evidence for the selective detection of Cu^{2+} (in addition to H^{+}) due to the coordination between the Nγ amino and the methoxy substituents as supported by the proton NMR titration studies. Furthermore, we demonstrated the practical utility of these azobenzene pH indicators on filter paper. We anticipate that these colorimetric azobenzene pH indicators will find many industrial applications in aqueous environments.

EXPERIMENTAL SECTION

The synthesis and characterization of **1** and **2** has been reported.[42] The synthesis and characterization of **3**−**5** have been reported.[31] Detailed experimental procedures and a comprehensive selection of NMR spectra for **3**−**5** are available in the Supporting Information.

ASSOCIATED CONTENT

Supporting Information

The Supporting Information is available free of charge on the ACS Publications website at DOI: 10.1021/acsomega.7b00887.

DOI: 10.1021/acsomega.7b00887
ACS Omega 2017, 2, 6159−6166

UV−vis absorption spectra and pH-absorbance profile of methyl yellow, pH-absorbance profile spectra of **5** with Cu^{2+}, UV−vis absorption spectra of **4** with Cu^{2+}; ^{1}H & ^{13}C NMR spectra, IR, and HRMS of **3**−**5**; ^{1}H NMR pD titration experiments of **3**−**5** and methyl yellow; $^{1}H-^{13}C$ gHMBC, $^{1}H-^{13}C$ gHSQC, $^{1}H-^{15}N$ gHMBC spectra of **3**−**5** at pD 1 and pD 4 (PDF)

AUTHOR INFORMATION

Corresponding Author

*E-mail: david.magri@um.edu.mt.

ORCID

David C. Magri: 0000-0002-6999-3667

Notes

The authors declare no competing financial interest.

ACKNOWLEDGMENTS

Financial support is acknowledged from the University of Malta, the Strategic Educational Pathways Scholarship (STEPS) part-financed by the European Social Fund (ESF) under Operational Programme II, and the European Cooperation in Science and Technology (COST Action CM1005 "Supramolecular Chemistry in Water"), the Slovenian Research Agency, the Ministry of Higher Education, Science and Technology of the Republic of Slovenia (program no. P1-0242) ENFIST Centre of Excellence. DFT calculations were performed at the Academic Computer Centre CYFRONET AGH within the computational grant "GRAPHENE" and were funded from the European Union's Horizon 2020 research and innovation programme under grant agreement No. 664786. Dr. Marina Kveder is acknowledged for valuable discussions.

REFERENCES

(1) Zollinger, H. *Color Chemistry. Syntheses, Properties, and Applications of Organic Dyes and Pigments*, 3rd ed.; Verlag Helvetica Chimica Acta: Zurich, 2003.

(2) Sabnis, R. W. *Handbook of Acid-Base Indicators*; CRC Press: Boca Raton, 2007.

(3) (a) Merino, E. *Chem. Soc. Rev.* **2011**, *40*, 3835−3853. (b) Bandara, H. M. D.; Burdette, S. C. *Chem. Soc. Rev.* **2012**, *41*, 1809−1825.

(4) Haberhauer, G.; Kallweit, C. *Angew. Chem., Int. Ed.* **2010**, *49*, 2418−2421.

(5) Baroncini, M.; d'Agostino, S.; Bergamini, G.; Ceroni, P.; Comotti, A.; Sozzani, P.; Bassanetti, I.; Grepioni, F.; Hernandez, T. M.; Silva, S.; Venturi, M.; Credi, A. *Nat. Chem.* **2015**, *7*, 634−640.

(6) Bushuyev, O. S.; Friščić, T.; Barrett, C. J. *CrystEngComm* **2016**, *18*, 7204−7211.

(7) Brown, J. W.; Henderson, B. L.; Kiesz, M. D.; Whalley, A. C.; Morris, W.; Grunder, S.; Deng, H.; Furukawa, H.; Zink, J. I.; Stoddart, J. F.; Yaghi, O. M. *Chem. Sci.* **2013**, *4*, 2858−2864.

(8) Gong, L. L.; Feng, X. F.; Luo, F. *Inorg. Chem.* **2015**, *54*, 11587−11589.

(9) Yeung, C. L.; Charlesworth, S.; Iqbal, P.; Bowen, J.; Preece, J. A.; Mendes, P. M. *Phys. Chem. Chem. Phys.* **2013**, *15*, 11014−11024.

(10) Ishikawa, D.; Ito, E.; Han, M.; Hara, M. *Langmuir* **2013**, *29*, 4622−4631.

(11) Wu, W.; Tang, R.; Lia, Q.; Li, Z. *Chem. Soc. Rev.* **2015**, *44*, 3997−4022.

(12) Yu, G.; Han, C.; Zhang, Z.; Chen, J.; Yan, X.; Zheng, B.; Liu, S.; Huang, F. *J. Am. Chem. Soc.* **2012**, *134*, 8711−8717.

(13) Abendroth, J. M.; Bushuyev, O. S.; Weiss, P. S.; Barrett, C. J. *ACS Nano* **2015**, *9*, 7746−7768.

(14) Osorio-Planes, L.; Espelt, M.; Pericas, M. A.; Ballester, P. *Chem. Sci.* **2014**, *5*, 4260−4264.

(15) Döbbelin, M.; Ciesielski, A.; Haar, S.; Osella, S.; Bruna, M.; Minoia, A.; Grisanti, L.; Mosciatti, T.; Richard, F.; Adi Prasetyanto, E.; De Cola, L.; Palermo, V.; Mazzaro, R.; Morandi, V.; Lazzaroni, R.; Ferrari, A. C.; Beljonne, D.; Samorì, P. *Nat. Commun.* **2016**, *7*, No. 11090.

(16) Deo, C.; Bogliotti, N.; Métivier, R.; Retailleau, P.; Xie, J. *Chem. − Eur. J.* **2016**, *22*, 9092−9096.

(17) Baroncini, M.; Ragazzon, G.; Silvi, S.; Venturi, M.; Credi, A. *Pure Appl. Chem.* **2015**, *87*, 537−545.

(18) Cheng, X.; Li, Q.; Li, C.; Qin, J.; Li, Z. *Chem. − Eur. J.* **2011**, *17*, 7276−7281.

(19) Kim, E.; Seo, S.; Seo, M. L.; Jung, J. H. *Analyst* **2010**, *135*, 149−156.

(20) Gunnlaugsson, T.; Leonard, J. P.; Murray, N. S. *Org. Lett.* **2004**, *6*, 1557−1560.

(21) Lee, S. J.; Lee, S. S.; Jeong, Y., II; Lee, J. Y.; Jung, J. H. *Tetrahedron Lett.* **2007**, *48*, 393−396.

(22) Debdas, R.; Bharadwaj, P. K. *Inorg. Chem.* **2008**, *47*, 2252−2254.

(23) (a) Hrishikesan, E.; Kannan, P. *Inorg. Chem. Commun.* **2013**, *37*, 21−25. (b) Hrishikesan, E.; Saravanan, C.; Kannan, P. *Ind. Eng. Chem. Res.* **2011**, *50*, 8225−8229.

(24) (a) Gunnlaugsson, T.; Nieuwenhuyzen, M.; Richard, L.; Thoss, V. *Tetrahedron Lett.* **2001**, *42*, 4725−4728. (b) Gunnlaugsson, T.; Nieuwenhuyzen, M.; Richard, L.; Thoss, V. *J. Chem. Soc., Perkin Trans. 2* **2002**, 141−150.

(25) Kaur, N.; Kumar, S. *Tetrahedron* **2011**, *67*, 9233−9264.

(26) Sareen, D.; Kaur, P.; Singh, K. *Coord. Chem. Rev.* **2014**, *265*, 125−154.

(27) Matazo, D. R. C.; Ando, R. A.; Borin, A. C.; Santos, P. S. *J. Phys. Chem. A* **2008**, *112*, 4437−4443.

(28) Kuroda, Y.; Lee, H.; Kuwae, A. *J. Phys. Chem.* **1980**, *84*, 3417−3423.

(29) Kuroda, Y.; Fujiwara, Y. *J. Phys. Chem.* **1981**, *85*, 2655−2659.

(30) Ferreira, I. R.; Ando, R. A. *Chem. Phys. Lett.* **2012**, *522*, 51−53.

(31) Cardona, M. A.; Magri, D. C. *Tetrahedron Lett.* **2014**, *55*, 4559−4563.

(32) Liwo, A.; Tempczyk, A.; Widernik, T.; Klentak, T.; Czermiński, J. *J. Chem. Soc., Perkin Trans. 2* **1994**, 71−75.

(33) Sawicki, E. *J. Org. Chem.* **1957**, *22*, 621−625.

(34) Sawicki, E. *J. Org. Chem.* **1957**, *22*, 915−919.

(35) Jaffe, H. H.; Yeh, S. J. *J. Org. Chem.* **1957**, *22*, 1281−1282.

(36) Zenhäusern, A.; Zollinger, H. *Helv. Chim. Acta* **1962**, *45*, 1890−1898.

(37) Farrugia, K. N.; Makuc, D.; Podborska, A.; Szaciłowski, K.; Plavec, J.; Magri, D. C. *Org. Biomol. Chem.* **2015**, *13*, 1662−1672.

(38) Farrugia, K. N.; Makuc, D.; Podborska, A.; Szaciłowski, K.; Plavec, J.; Magri, D. C. *Eur. J. Org. Chem.* **2016**, *2016*, 4415−4422.

(39) Makuc, D.; Lenarčič, M.; Bates, G. W.; Gale, P. A.; Plavec, J. *Org. Biomol. Chem.* **2009**, *7*, 3505−3511.

(40) Makuc, D.; Albrecht, M.; Plavec, J. *Supramol. Chem.* **2010**, *22*, 603−611.

(41) Makuc, D.; Hiscock, J. R.; Light, M. E.; Gale, P. A.; Plavez, J. *Beilstein J. Org. Chem.* **2011**, *7*, 1205−1214.

(42) Cardona, M. A.; Kveder, M.; Baisch, U.; Probert, M. R.; Magri, D. C. *RSC Adv.* **2016**, *6*, 84712−84721.

(43) Cardona, M. A.; Mallia, C. J.; Baisch, U.; Magri, D. C. *RSC Adv.* **2016**, *6*, 3783−3791.

(44) Bingol, H.; Kocabas, E.; Zor, E.; Coskun, A. *Talanta* **2010**, *82*, 1538−1542.

(45) Martin, G. J.; Martin, M. L.; Gouesnard, J.-P. *^{15}N-NMR Spectroscopy*; Springer: New York, 1981.

(46) Marek, R.; Lyčka, A.; Kolehmainen, E.; Sievänen, E.; Toušek, J. *Curr. Org. Chem.* **2007**, *11*, 1154−1205.

(47) Lambert, J. B.; Binsch, G.; Roberts, J. D. *Proc. Natl. Acad. Sci. U.S.A.* **1964**, *51*, 735−737.

(48) Klamt, A.; Moya, C.; Palomar, J. *J. Chem. Theory Comput.* **2015**, *11*, 4220−4225.

DOI: 10.1021/acsomega.7b00887
ACS Omega 2017, 2, 6159−6166